IEEE Access
Multidisciplinary ⋮ Rapid Review ⋮ Open Access Journal

Date of publication xxxx 00, 0000, date of current version xxxx 00, 0000.
Digital Object Identifier 10.1109/ACCESS.2017.Doi Number

A General Dynamic State Estimation Framework for Monitoring and Control of Permanent Magnetic Synchronous Generators-Based Wind Turbines

Shaojian Song[1], Member, IEEE, Panzhou Wu[1], Yuzhang Lin[2], Member, IEEE, and Yanbo Chen[3], Senior Member, IEEE

[1] School of Electrical Engineering, Guangxi University, Nanning 530004, China
[2] Department of Electrical and Computer Engineering, University of Massachusetts, Lowell, MA 01854, USA
[3] School of Electrical & Electronic Engineering, North China Electric Power University, Beijing 102206, China

Corresponding author: Yuzhang Lin (e-mail: yuzhang_lin@uml.edu).

ABSTRACT Existing Dynamic State Estimation (DSE) techniques for Permanent Magnetic Synchronous Generators-based Wind Turbines (PMSG-WTs) are impractical as they blend the physical dynamics of PMSG-WTs (i.e. *plants*) with the digital dynamics of the *controllers*. In this paper, a general DSE framework for PMSG-WT monitoring and control is proposed, which decouples the *plant* model from the *controller* model. Based on the decoupled models, the state transition equations and measurement equations of the *plant* are derived respectively. Then, based on the equivalence between the correction stage of iterated extended Kalman filtering (IEKF) and the weighted least squares (WLS) regression, a DSE algorithm that can effectively filter out noise and bad data is presented. Simulation results in the IEEE 39-bus system show that the DSE improves the accuracy of state trajectory monitoring than the raw measurements by 64.9%-78.4% and the accuracy of control setpoint tracking by 25.5%-33.9%.

INDEX TERMS Permanent Magnetic Synchronous Generators, Dynamic State Estimation, Kalman Filtering, Situational Awareness, Power System Control, Wind Generation

I. INTRODUCTION

The penetration of wind generation is rapidly increasing in power systems around the world [1-2]. Over the years, Permanent Magnetic Synchronous Generators-based Wind Turbines (PMSG-WTs) have gradually become one of the dominating type of wind generation systems. In order to ensure the stable and efficient operation of power systems, it is critical to monitor and control PMSG-WTs accurately and reliably in real time.

Dynamic State Estimation (DSE) is an essential tool for the monitoring and control of power and energy systems [3-4]. A key driver of the DSE technology is the wide deployment of Phasor Measurement Units (PMUs), which makes it possible to observe power system operation trajectories in a finer time scale and in a synchronous fashion [5-6]. Existing approaches on DSE can be broadly divided into two categories. The first category is the widely used Kalman Filtering (KF) techniques. Typical methods under this category are Extended Kalman Filter (EKF), Unscented Kalman Filter (UKF), and Cubature Kalman filter (CKF). As power systems are generally nonlinear, EKF are naturally considered for DSE [7-9], which linearize nonlinear functions by preserving the first order term of the Taylor series expansion. In order to reduce the estimation error induced by linearization, DSE techniques based on UKF are proposed, which has stronger adaptability to system nonlinearity [10-11]. Recently, CKF using volume transformation are applied for DSE in [12-13], which further improves the accuracy and robustness in strongly nonlinear environment. The second category of methods is the Particle Filtering (PF) technique. It can achieve high estimation accuracy under both Gaussian and non-Gaussian noises, but comes at the cost of higher computational burden [14-16]. Besides centralized solutions, decentralized techniques have also been proposed. Compared with the centralized algorithms, Distributed Particle Filter (DPF) manifests better tracking accuracy and robustness in dynamic environment [17-18].

In the existing literature, a vast majority of works target the traditional synchronous generators [5-6], while the DSE of wind generators requires further investigation [19]. Refs. [20-22] use UKF to estimate the dynamic state of Doubly Fed Induction Generator based Wind Turbines (DFIG-WTs). Refs. [23] and [24] use EKF and Ensemble Kalman Filter (EnKF) to estimate the dynamic state of PMSG-WTs, respectively. In these only existing publications on the DSE of PMSG-WTs [23-24], a major limitation is presented: the physical wind generation system model (i.e. the "*plant*" model in control theory) and the *controller* model are blended in the estimation process, which results in the following problems. (1) The physical variables in the *plant* model and the digital variables in the *controller* are denoted by the same set of variables. In reality, however, these two sets of variables are not identical, in that both the sensing process (from the physical world to the

Nomenclature

x	state vector	V_g	voltage of grid-side filter
z	measurement vector	R_f	resistance of grid-side filter
u	input vector	L_f	inductance of grid-side filter
c	control signal	Q_s	generator-side reactive power
w	process error vector	Q_g	grid-side reactive power
v	measurement error vector	P_s	generator-side active power
P	covariance matrix of estimate error	P_g	grid-side active power
Q	covariance matrix of process error	C	capacitance of DC bus
R	covariance matrix of measurement error	V_{DC}	DC-link voltage
r	estimated residual	α	shaft twist angle
G	gain matrix	ω_t	wind turbine speed
i_s	stator current	ω_g	rotor speed
V_s	stator voltage	ω_s	electrical angular velocity of grid voltage
R_s	stator resistance	H_g	inertia constants of generator
L_s	stator inductance	H_t	inertia constants of wind turbine
ψ_{pm}	permanent magnet flux	K_s	shaft stiffness coefficient
i_g	output current of grid-side converter	D	damping coefficient
V_c	output voltage of grid-side converter	T_m	wind turbine torque
M	intermediate state variable	C_p	wind energy coefficient
		λ	tip speed ratio

digital world) and the actuation process (from the digital world to the physical world) are imperfect. For example, the actual currents in the machine stator may be different from the measured values fed into the controller due to measurement errors; and the voltage signals output from the controller may be different from the actual voltages across the machine terminals due to the actuation imperfection. Failing to consider the uncertainty between the physical world and the digital world will inevitably lead to degraded estimator performances in practice. (2) While the physical model of PMSG-WTs is relatively fixed, a variety of control algorithms can be applied, which will drastically change the controller model. Thus, the blended model proposed in [23-24] is not generally applicable to PMSG-WTs with different types of controllers. It should be noted that some existing work already implements the principle of decoupling for wind turbines [25], but only for the mechanical part of the system, and not for the entire electro-mechanical system and the DSE application.

In order to overcome the aforementioned problems in the existing literature, this paper proposes a general DSE framework that separates the *plant* model from the *controller* model, and explicitly distinguishes the physical variables in the *plant* model from the digital variables in the *controller* model. A Weighted-Least-Square-form Iterated Extended Kalman Filter (WLS-form IEKF) based on the equivalence between the correction stage of IEKF and the WLS regression [26-27] is then proposed to allow convenient detection, identification, and correction of bad data using the Largest Normalized Residual (LNR) test [28-30]. Two alternative DSE schemes, i.e. the open-loop scheme for system monitoring, and the closed-loop scheme for system control are also presented. In summary, the proposed DSE framework for PMSG-WT has the following features that the existing works do not have:

(1) The DSE framework accounts for the uncertainties of measurements and control signals by separately modeling the *plant* and the *controller* of PMSG-WTs, and explicitly describing the information exchange processes between them.

(2) The DSE framework is generally applicable to PMSG-WTs with various control algorithms. As the digital variables in the *controller* are known, the DSE aims to track the physical variables in the *plant* only. Consequently, the replacement of control algorithms does not affect the applicability of the proposed framework.

(3) The DSE framework can effectively monitor and control PMSG-WT system in the presence of noise, natural bad data, or maliciously injected false data, significantly enhancing the robustness of system monitoring and control.

The rest of paper is organized as follows: Section II briefly introduces the dynamic model of a grid-connected PMSG-WT system. Notably, the system model is divided into the *plant* model and *controller* model. The information exchange processes between them are explicitly considered, and the variables associated with them are separately defined. Section III introduces the proposed DSE framework, where the state and measurement equations are derived, and the detailed WLS-form IEKF estimation procedure is described. The two operation schemes for system monitoring and control are also presented. Comprehensive simulation results under different types of uncertainties and operation schemes are presented and discussed in Section IV. Section V summarizes the observations and concludes the paper.

II. STATE SPACE MODEL OF GRID-CONNECTED PMSG-WT

PMSG-WTs are widely deployed today due to their low maintenance cost, flexible speed control capability, and full reactive power control capability [31-32]. The complete nonlinear dynamic model of a grid-connected PMSG-WT includes the wind turbine, the PMSG, the generator-side converter, the DC link, the grid-side converter, the grid-side filter, as well as converter controllers. In this section, the model is divided into the *plant* model (physical world) and *controller* model (digital world). Both of them are dynamic systems described by differential equations.

A. PLANT MODEL

The *plant* of PMSG-WT entails the physical wind generation

system including the wind turbine, the PMSG, the generator-side converter, the DC link, the grid-side converter, and the grid-side filter [33-34]. In this subsection, and the dynamic equations constituting the plant model will be presented, where the superscript "c" denotes the control signal inputs that the *controller* feeds to the *plant*.

The dynamic equations of stator current in the d-q reference frame can be written as follows:

$$\frac{d}{dt}i_{sd}=\frac{\omega_b}{L_{sd}}\left(-V_{sd}^{c}-R_s i_{sd}+\omega_g L_{sq} i_{sq}\right), \tag{1}$$

$$\frac{d}{dt}i_{sq}=\frac{\omega_b}{L_{sq}}\left(-V_{sq}^{c}-R_s i_{sq}-\omega_g L_{sd} i_{sd}+\omega_g \psi_{pm}\right), \tag{2}$$

where the subscripts "d" and "q" denote variables in the d axis and the q axis, respectively; V_s and i_s represent the stator voltage and the stator current of the PMSG, respectively; L_s and R_s represent the stator inductance and the stator resistance, respectively; ω_g and ψ_{pm} represent the rotor speed and the permanent magnet flux, respectively.

The dynamic equations of the output current of the grid-side filter in the d-q reference frame are given as follows:

$$\frac{d}{dt}i_{gd}=\frac{\omega_b}{L_f}\left(V_{cd}^{c}-R_f i_{gd}+\omega_s L_f i_{gq}-V_{gd}\right), \tag{3}$$

$$\frac{d}{dt}i_{gq}=\frac{\omega_b}{L_f}\left(V_{cq}^{c}-R_f i_{gq}-\omega_s L_f i_{gd}-V_{gq}\right), \tag{4}$$

where V_c and i_g represent the output voltage and current of grid-side converter, respectively; L_f and R_f represent the inductance and resistance of grid-side filter, respectively; V_g and ω_s represent the voltage of the grid-side filter and the electrical angular velocity of the grid voltage, respectively.

In the DC link, the dynamics of DC voltage can be described by the following equation:

$$\frac{d}{dt}V_{DC}=\frac{1}{CV_{DC}}\left(V_{sd}i_{sd}+V_{sq}i_{sq}-V_{gd}i_{gd}-V_{gq}i_{gq}\right), \tag{5}$$

where V_{DC} is the DC-link voltage, and C is the capacitance of DC bus.

The mechanical drive train includes the turbine, the blades, bearing, and other mechanical components. The equations to collectively describe the mechanical dynamics are as follows:

$$\frac{d\alpha}{dt}=\omega_t-\omega_g, \tag{6}$$

$$\frac{d}{dt}\omega_t=\frac{1}{2H_t}\left[T_m-K_s\alpha-D\left(\omega_t-\omega_g\right)\right], \tag{7}$$

$$\frac{d}{dt}\omega_g=\frac{1}{2H_g}\left\{-\left[\left(L_{sq}-L_{sd}\right)i_{sd}+\psi_{pm}\right]i_{sq}+K_s\alpha+D\left(\omega_t-\omega_g\right)\right\}, \tag{8}$$

where α and ω_t represent the shaft twist angle and the wind turbine speed, respectively; K_s and D represent the shaft stiffness coefficient and the damping coefficient respectively; H_g and H_t refer to the inertia constants of the generator and the wind turbine, respectively. The wind turbine torque T_m depends on the wind speed v_w. However, in order to achieve Maximum Power Point Tracking (MPPT), the wind turbine speed ω_t under the optimal tip speed ratio is computed according to the real-time measured wind speed signal [35-36], then, the generator speed is adjusted to track the optimal speed setpoint ω_{gref} so as to achieve MPPT.

The relationships are described as follows:

$$T_m=\frac{P_m}{\omega_t}=\frac{1}{2\omega_t}\rho\cdot A\cdot C_p\cdot v_w^3, \tag{9}$$

$$\lambda=\frac{\omega_t R}{v_w}. \tag{10}$$

where ρ, A , C_p , R , λ , P_m are air density, swept area, wind energy coefficient, blade radius, tip speed ratio and turbine output power, respectively.

B. CONTROLLER MODEL

The controller model consists of the generator-side controller and the grid-side controller. Ref. [23] describes one of the common control paradigm, where the generator-side controller is used to control the DC-link voltage and the reactive power injected into the generator, and the grid-side converter is used to control the active and reactive powers injected into the grid. However, it does not distinguish the digital variables in the *controller* and the physical variables in the *plant*, thus failing to consider the inherent uncertainties in the information exchange processes (i.e. sensing and actuation) between the *plant* and the *controller*. In this paper, the *controller* will be separately modeled. Variables with the superscript "z" clearly denotes the measurements that the *plant* feeds to the *controller*.

The outer-loop control on the generator side tracks the setpoint of the generator-side reactive power Q_{sref} and the setpoint of the DC-link voltage V_{DCref}, as is shown in Fig. 1a. K_{pn} (n=1,…,8) and K_{in} (n=1,…,8) are the proportional coefficient and integral coefficient of proportional-integral (PI) controller respectively. The dynamics of the intermediate state variables M_2 and M_4 of the outer-loop controller are described as follows:

$$\frac{dM_2}{dt}=K_{i1}\left(Q_{sref}-V_{sq}^{z}i_{sd}^{z}+V_{sd}^{z}i_{sq}^{z}\right), \tag{11}$$

$$\frac{dM_4}{dt}=K_{i3}\left(V_{DCref}-V_{DC}^{z}\right). \tag{12}$$

The inner-loop control on the generator side tracks the setpoint of the stator currents i_{sdref} and i_{sqref} from outer loop, as also shown in Fig. 1a. The dynamics of the intermediate state variables M_1 and M_3 of the inner-loop control are described as follows:

$$\frac{dM_1}{dt}=K_{i2}\left[K_{p1}\left(Q_{sref}-V_{sq}^{z}i_{sd}^{z}+V_{sd}^{z}i_{sq}^{z}\right)+M_2-i_{sd}^{z}\right], \tag{13}$$

$$\frac{dM_3}{dt}=K_{i4}\left[K_{p3}\left(V_{DCref}-V_{DC}^{z}\right)+M_4-i_{sq}^{z}\right]. \tag{14}$$

The outer-loop control on the grid side tracks the setpoint of the reactive power on the grid side Q_{gref} and the setpoint of generator speed ω_{gref} from the MPPT process, as shown in Fig. 1b. The dynamics of the intermediate state variables M_6 and M_8 in the outer-loop control are described as follows:

$$\frac{dM_6}{dt}=K_{i5}\left(\omega_{gref}-\omega_g^{z}\right), \tag{15}$$

$$\frac{dM_8}{dt}=K_{i7}\left(Q_{gref}-V_{gq}^{z}i_{gd}^{z}+V_{gd}^{z}i_{gq}^{z}\right). \tag{16}$$

The inner-loop control on the grid side tracks the setpoint of the grid currents i_{gdref} and i_{gqref} from the outer loop, as also shown in Fig. 1b. The dynamics of the intermediate state variables M_5 and M_7 in the inner-loop control are described as follows:

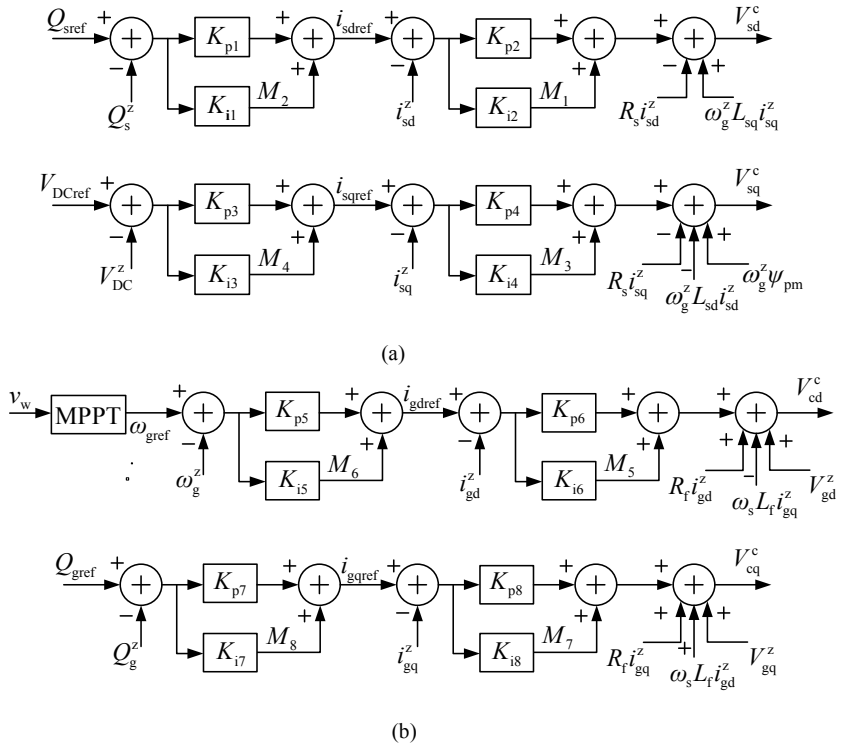

FIGURE 1. **Controller model. (a) Generator-side converter controller; (b) Grid-side converter controller.**

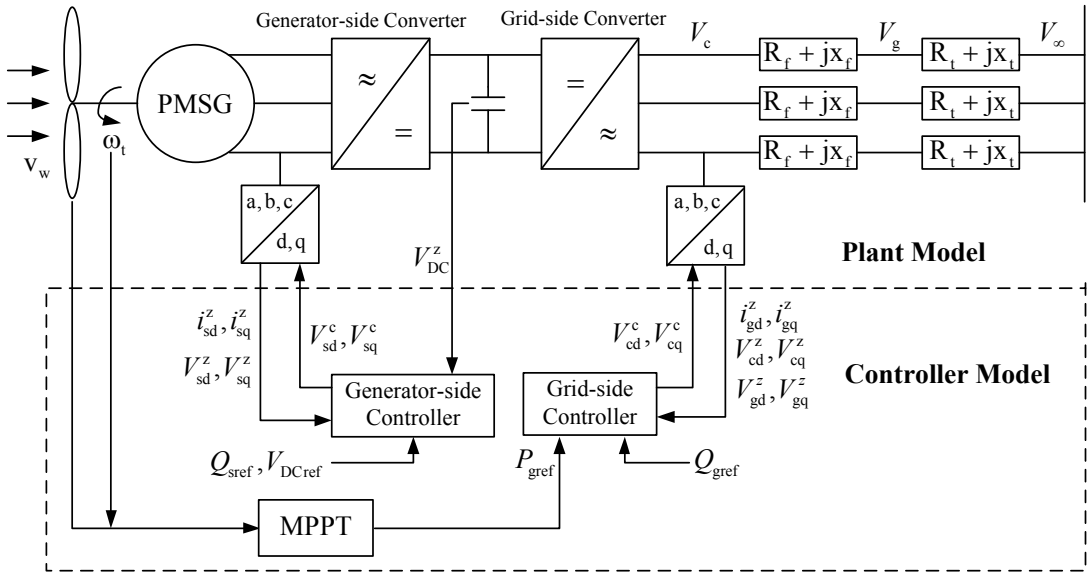

FIGURE 2. **Plant-controller breakdown of PMSG-WT.**

$$\frac{dM_5}{dt} = K_{i6}\left[K_{p5}\left(\omega_{gref} - \omega_g^z\right) + M_6 - i_{gd}^z\right], \tag{17}$$

$$\frac{dM_7}{dt} = K_{i8}\left[K_{p7}\left(Q_{gref} - V_{gq}^z i_{gd}^z + V_{gd}^z i_{gq}^z\right) + M_8 - i_{gq}^z\right]. \tag{18}$$

It should be noted that the control algorithms of PMSG-WTs are far from unique, and (11)-(18) only represent one common algorithm. In the case of other control algorithms, the dynamic equations should also be changed. However, as the *plant* and the *controller* are considered separately in this paper, the change of the *controller* type does not affect the proposed DSE framework.

C. INTERACTION BETWEEN THE PLANT MODEL AND THE CONTROLLER MODE

The physical state variables in the *plant* model can be defined as $\mathbf{x} = [i_{sd}, i_{sq}, i_{gd}, i_{gq}, V_{DC}, \alpha, \omega_g, \omega_t]^T$, while the digital state variables in *controller* model can be defined as $\mathbf{m} = [M_1, M_2, M_3, M_4, M_5, M_6, M_7, M_8]^T$. The information exchange between the two models is illustrated in Fig. 2. Denote the vector of

measurement signals and the vector of control signals as **z** and **c** respectively, then they can be written as:

$$\mathbf{z}=\left[i_{sd}^{z},i_{sq}^{z},i_{gd}^{z},i_{gq}^{z},V_{DC}^{z},\omega_{g}^{z},V_{sd}^{z},V_{sq}^{z},V_{gd}^{z},V_{gq}^{z},V_{cd}^{z},V_{cq}^{z},Q_{S}^{z},Q_{g}^{z},P_{S}^{z},P_{g}^{z}\right]^{\mathrm{T}} \quad (19)$$

$$\mathbf{c}=\left[V_{sd}^{c},V_{sq}^{c},V_{cd}^{c},V_{cq}^{c}\right]^{\mathrm{T}}. \quad (20)$$

As can be seen, the *controller* needs to collect the measurement from the *plant*, and returns control signals to the *plant*, forming a complete closed loop. Because the *plant* model and the *controller* model are blended in previous publications [23-24], the measurements **z**, and the control signals **c**, and the actual state variables in the *plant* and the *controller* cannot be distinguished. For example, V_{sd}^{c} is a control signal of V_{sd}, while V_{sd}^{z} is a measurement of V_{sd}. The differences between V_{sd}^{c}, V_{sd}^{z}, and V_{sd} are always present in reality due to the uncertainties of the sensing and actuation processes. Denoting them as the same variable as in [23-24] implicitly ignores these differences, and limits the capability of the DSE algorithm for handling these uncertainties.

III. DYNAMIC STATE ESTIMATION OF PMSG-WT

The previous section develops the *plant* model and the *controller* model of PMSG-WTs separately. As is obvious, the digital variables in the *controller* are perfectly known and do not need to be estimated, thus it is only necessary to estimate the physical state variables in the *plant* model. This feature is fundamentally different from the existing publications [23-24] and enables the development of a general DSE framework for PMSG-WTs with various control algorithms.

A. STATE TRANSITION EQUATIONS AND MEASUREMENT EQUATIONS

As PMSG-WT is a typical dynamic nonlinear system, the state transition equations and measurement equations can be described as follows:

$$\mathbf{x}_{k}=\boldsymbol{f}_{k\text{-}1}\left(\mathbf{x}_{k\text{-}1},\mathbf{u}_{k\text{-}1}\right)+\mathbf{w}_{k\text{-}1}, \quad (21)$$

$$\mathbf{z}_{k}=\boldsymbol{h}_{k}\left(\mathbf{x}_{k}\right)+\mathbf{v}_{k}. \quad (22)$$

where $\boldsymbol{f}$ and $\boldsymbol{h}$ represent the state transition function and measurement function, respectively; **x** and **z** are the state vector and the measurement vector respectively; **w** and **v** are the vectors of process noise and measurement noise, respectively, both of which are assumed to be Gaussian white. Based on (1)-(8), the discretized state transition equations are presented in (23)-(30), where T_s is the sampling period, and superscript "w" represents the process noise of each state variable.

$$\begin{aligned}i_{sd}(k+1)&=\frac{T_s\omega_b}{L_{sd}}\left[-V_{sq}^{c}(k)+\omega_g(k)L_{sq}i_{sq}(k)\right]\\&+\left(1-\frac{T_s\omega_b R_s}{L_{sd}}\right)i_{sd}(k)+i_{sd}^{w}(k),\end{aligned} \quad (23)$$

$$\begin{aligned}i_{sq}(k+1)&=\frac{T_s\omega_b}{L_{sq}}\left[-V_{sq}^{c}(k)-\omega_g(k)L_{sd}i_{sd}(k)+\omega_g(k)\psi_{pm}\right]\\&+\left(1-\frac{T_s\omega_b R_s}{L_{sq}}\right)i_{sq}(k)+i_{sq}^{w}(k),\end{aligned} \quad (24)$$

$$\begin{aligned}i_{gd}(k+1)&=\frac{T_s\omega_b}{L_f}\left[V_{cd}^{c}(k)+\omega_s L_f i_{gq}(k)-V_{gd}^{z}(k)\right]+i_{gd}^{w}(k)\\&+\left(1-\frac{T_s\omega_b R_f}{L_f}\right)i_{gd}(k),\end{aligned} \quad (25)$$

$$\begin{aligned}i_{gq}(k+1)&=\frac{T_s\omega_b}{L_f}\left[V_{cq}^{c}(k)-\omega_s L_f i_{gd}(k)-V_{gq}^{z}(k)\right]+i_{gq}^{w}(k)\\&+\left(1-\frac{T_s\omega_b R_f}{L_f}\right)i_{gq}(k),\end{aligned} \quad (26)$$

$$\begin{aligned}V_{DC}(k+1)&=V_{DC}(k)+\frac{T_s}{CV_{DC}(k)}\left[V_{sd}^{c}(k)i_{sd}(k)+V_{sq}^{c}(k)i_{sq}(k)\right.\\&\left.-V_{gd}^{z}(k)i_{gd}(k)-V_{gq}^{z}(k)i_{gq}(k)\right]+V_{DC}^{w}(k),\end{aligned} \quad (27)$$

$$\alpha(k+1)=\alpha(k)+T_s\omega_b\left[\omega_t(k)-\omega_g(k)\right]+\alpha^{w}(k) \quad (28)$$

$$\begin{aligned}\omega_g(k+1)&=\left(1-\frac{T_s D}{2H_g}\right)\omega_g(k)+\frac{T_s\left[K_s\alpha(k)+D\omega_t(k)\right]}{2H_g}\\&+\frac{T_s\left[-(L_{sq}-L_{sd})i_{sd}(k)i_{sq}(k)-\psi_{pm}i_{sq}(k)\right]}{2H_g}+\omega_g^{w}(k),\end{aligned} \quad (29)$$

$$\begin{aligned}\omega_t(k+1)&=\frac{T_s\left[T_m-K_s\alpha(k)+D\omega_t(k)\right]}{2H_t}\\&+\left(1-\frac{T_s D}{2H_t}\right)\omega_t(k)+\omega_t^{w}(k).\end{aligned} \quad (30)$$

In order to estimate the above state variables, measurement equations are needed, which are presented in (31)-(44), where the superscript "v" denotes the measurement noise:

$$i_{sd}^{z}(k)=i_{sd}(k)+i_{sd}^{v}, \quad (31)$$

$$i_{sq}^{z}(k)=i_{sq}(k)+i_{sq}^{v}, \quad (32)$$

$$i_{gd}^{z}(k)=i_{gd}(k)+i_{gd}^{v}, \quad (33)$$

$$i_{gq}^{z}(k)=i_{gq}(k)+i_{gq}^{v}, \quad (34)$$

$$V_{DC}^{z}(k)=V_{DC}(k)+V_{DC}^{v}, \quad (35)$$

$$\omega_{g}^{z}(k)=\omega_{g}(k)+\omega_{g}^{v}, \quad (36)$$

$$\begin{aligned}V_{sd}^{z}(k)&=\frac{L_{sd}}{T_s\omega_b}i_{sd}(k-1)-\left(\frac{L_{sd}}{T_s\omega_b}+R_s\right)i_{sd}(k)\\&+\omega_g(k)L_{sq}i_{sq}(k)+V_{sd}^{v}+i_{sd}(k-1)^{w},\end{aligned} \quad (37)$$

$$\begin{aligned}V_{sq}^{z}(k)&=\frac{L_{sq}}{T_s\omega_b}i_{sq}(k-1)-\left(\frac{L_{sq}}{T_s\omega_b}+R_s\right)i_{sq}(k)+\omega_g(k)\psi_{pm}\\&-\omega_g(k)L_{sd}i_{sd}(k)+V_{sq}^{v}+i_{sq}(k-1)^{w},\end{aligned} \quad (38)$$

$$\begin{aligned}V_{cd}^{z}(k)&=\left(R_f+\frac{L_f}{T_s\omega_b}\right)i_{gd}(k)-\frac{L_f}{T_s\omega_b}i_{gd}(k-1)-\omega_s L_f i_{gq}(k)\\&+V_{gd}^{z}(k)+V_{cd}^{v}+i_{gd}(k-1)^{w},\end{aligned} \quad (39)$$

$$\begin{aligned}V_{cq}^{z}(k)&=\left(R_f+\frac{L_f}{T_s\omega_b}\right)i_{gq}(k)-\frac{L_f}{T_s\omega_b}i_{gq}(k-1)+\omega_s L_f i_{gd}(k)\\&+V_{gq}^{z}(k)++V_{cq}^{v}+i_{gq}(k-1)^{w},\end{aligned} \quad (40)$$

$$Q_{s}^{z}(k)=V_{sq}^{z}(k)i_{sd}(k)-V_{sd}^{z}(k)i_{sq}(k)+Q_{s}^{v}, \quad (41)$$

$$Q_{g}^{z}(k)=V_{gq}^{z}(k)i_{gd}(k)-V_{gd}^{z}(k)i_{gq}(k)+Q_{g}^{v}, \quad (42)$$

$$P_{s}^{z}(k)=V_{sd}^{z}(k)i_{sd}(k)+V_{sq}^{z}(k)i_{sq}(k)+P_{s}^{v}, \quad (43)$$

$$P_{g}^{z}(k)=V_{gd}^{z}(k)i_{gd}(k)+V_{gq}^{z}(k)i_{gq}(k)+P_{g}^{v}. \quad (44)$$

B. DYNAMIC STATE ESTIMATION

KF is a common method of DSE in power systems. In this paper, a WLS-form IEKF will be presented based on the equivalence between the correction stage of IEKF and the WLS regression. This formulation allows convenient application of the LNR method for bad data detection, identification, and correction [28-30]. The vector of state variables in a PMSG-WT system (i.e. the *plant* model) can be expressed as follows:

$$\mathbf{x}=\left[i_{\mathrm{sd}},i_{\mathrm{sq}},i_{\mathrm{gd}},i_{\mathrm{gq}},V_{\mathrm{DC}},\alpha,\omega_{\mathrm{g}},\omega_{\mathrm{t}}\right]^{\mathrm{T}}. \tag{45}$$

The measurement vector **z** can be expressed as follows:

$$\mathbf{z}=\left[i_{\mathrm{sd}}^{z},i_{\mathrm{sq}}^{z},i_{\mathrm{gd}}^{z},i_{\mathrm{gq}}^{z},V_{DC}^{z},\omega_{\mathrm{g}}^{z},V_{\mathrm{sd}}^{z},V_{\mathrm{sd}}^{z},V_{\mathrm{sq}}^{z},V_{\mathrm{gd}}^{z},V_{\mathrm{gq}}^{z},V_{\mathrm{cd}}^{z},V_{\mathrm{cq}}^{z},Q_{\mathrm{s}}^{z},Q_{\mathrm{g}}^{z},P_{\mathrm{s}}^{z},P_{\mathrm{g}}^{z}\right]^{\mathrm{T}}, \tag{46}$$

The vectors of inputs **u** can be expressed as follows:

$$\mathbf{u}=\left[Q_{\mathrm{sref}},Q_{\mathrm{gref}},V_{\mathrm{DCref}},v_{\mathrm{w}},V_{\infty}\right]^{\mathrm{T}}. \tag{47}$$

The specific steps for estimating the state of a PMSG-WT are summarized as follows.

(1) Set time step $t = 0$. Initialize the posteriori estimate of state variables $\hat{\mathbf{x}}_{t(+)}$, and the covariance matrix of the posteriori estimate of dynamic state variables $\mathbf{P}_{t(+)}$.

(2) Set $t \leftarrow t+1$.

(3) Prediction stage. The priori estimate of the dynamic state variables $\hat{\mathbf{x}}_{t(-)}$ can be predicted by the state transition equations at time t as follows:

$$\hat{\mathbf{x}}_{t(-)}=\boldsymbol{f}_{t-1}\left(\hat{\mathbf{x}}_{t-1},\mathbf{u}_{t-1}\right), \tag{48}$$

where $\boldsymbol{f}$ is derived from (23)-(30).

(4) The covariance matrix of the priori estimate is evaluated as follows:

$$\mathbf{P}_{t(-)}=\mathbf{F}_{t-1}\mathbf{P}_{t-1}\mathbf{F}_{t-1}^{T}+\mathbf{Q}_{t-1}, \tag{49}$$

where **F** is Jacobian matrix of $\boldsymbol{f}$, and **Q** is covariance matrix of process noise.

(5) Correction stage. Solve the following WLS problem, which is equivalent to the correction stage of standard IEKF [26-27]:

$$\begin{aligned}\hat{\mathbf{x}}_{t(+)}=\arg\min_{\mathbf{x}_t}&\left\{\left(\mathbf{z}_t-\mathbf{h}_t\left(\mathbf{x}_t\right)\right)^{T}\mathbf{R}_t^{-1}\left(\mathbf{z}_t-\mathbf{h}_t\left(\mathbf{x}_t\right)\right)\right.\\&\left.+\left(\hat{\mathbf{x}}_{t(-)}-\mathbf{x}_t\right)^{T}\mathbf{P}_{t(-)}^{-1}\left(\hat{\mathbf{x}}_{t(-)}-\mathbf{x}_t\right)\right\}\end{aligned} \tag{50}$$

which can be written equivalently in the following form:

$$\begin{aligned}\hat{\mathbf{x}}_{t(+)}&=\arg\min_{\mathbf{x}_t}\left\{\left(\begin{bmatrix}\mathbf{z}_t\\ \hat{\mathbf{x}}_{t(-)}\end{bmatrix}-\begin{bmatrix}\mathbf{h}_t\left(\mathbf{x}_t\right)\\ \mathbf{x}_t\end{bmatrix}\right)^{T}\begin{bmatrix}\mathbf{R}_t & \\ & \mathbf{P}_{t(-)}\end{bmatrix}^{-1}\left(\begin{bmatrix}\mathbf{z}_t\\ \hat{\mathbf{x}}_{t(-)}\end{bmatrix}-\begin{bmatrix}\mathbf{h}_t\left(\mathbf{x}_t\right)\\ \mathbf{x}_t\end{bmatrix}\right)\right\}\\&=\arg\min_{\mathbf{x}_t}\left(\tilde{\mathbf{z}}_t-\tilde{\mathbf{h}}_t\left(\mathbf{x}_t\right)\right)^{T}\tilde{\mathbf{R}}_t^{-1}\left(\tilde{\mathbf{z}}_t-\tilde{\mathbf{h}}_t\left(\mathbf{x}_t\right)\right)\end{aligned} \tag{51}$$

where $\tilde{\mathbf{z}}_t=\left(\mathbf{z}_t^{T},\hat{\mathbf{x}}_{t(-)}^{T}\right)^{T}$, $\tilde{\mathbf{h}}_t\left(\mathbf{x}_t\right)=\left(\mathbf{h}_t\left(\mathbf{x}_t\right)^{T},\mathbf{x}_t^{T}\right)^{T}$ and $\tilde{\mathbf{R}}_t=diag\left(\mathbf{R}_t,\mathbf{P}_{t(-)}\right)$. The Gauss-Newton method can be used for solving this problem. Specific steps are given as follows.

(5.1) Set iteration number $k = 0$. Initialize state variables $\mathbf{x}_{k,t}$, set the state estimate tolerance $\tau > 0$, and bad data detection threshold $c > 0$.

(5.2) The Jacobian matrix and the gain matrix are evaluated as follows:

$$\tilde{\mathbf{H}}_{k,t}\left(\mathbf{x}_{k,t}\right)=\frac{\partial\tilde{\mathbf{h}}_{k,t}\left(\mathbf{x}_{k,t}\right)}{\partial\mathbf{x}_{k,t}}, \tag{52}$$

$$\tilde{\mathbf{G}}_{k,t}\left(\mathbf{x}_{k,t}\right)=\tilde{\mathbf{H}}_{k,t}^{T}\left(\mathbf{x}_{k,t}\right)\tilde{\mathbf{R}}_{k,t}^{-1}\tilde{\mathbf{H}}_{k,t}\left(\mathbf{x}_{k,t}\right), \tag{53}$$

where **R** is covariance matrix of measurement noise.

(5.3) The state update vector is evaluated as follows:

$$\Delta\mathbf{x}_{k,t}=\tilde{\mathbf{G}}_{k,t}\left(\mathbf{x}_{k,t}\right)^{-1}\tilde{\mathbf{H}}_{k,t}^{T}\left(\mathbf{x}_{k,t}\right)\mathbf{R}_{k,t}^{-1}\left[\tilde{\mathbf{z}}_{k,t}-\tilde{\mathbf{h}}_{k,t}\left(\mathbf{x}_{k,t}\right)\right]. \tag{54}$$

(5.4) Keep updating the state estimate vector by

$$\mathbf{x}_{k+1,t}=\mathbf{x}_{k,t}+\Delta\mathbf{x}_{k,t}. \tag{55}$$

(5.5) If $\left|\Delta\mathbf{x}_{k,t}\right|>\tau$, set $k \leftarrow k+1$, and return to Step (5.2); Otherwise, set $\hat{\mathbf{x}}_{t(+)}=\mathbf{x}_{k,t}$ and $\tilde{\mathbf{H}}_t=\tilde{\mathbf{H}}_{k,t}$, and proceed to Step (6).

(6) The covariance matrix of the state estimate is evaluated as follows:

$$\mathbf{P}_{t(+)}=\left(\tilde{\mathbf{H}}_t^{T}\tilde{\mathbf{R}}_t^{-1}\tilde{\mathbf{H}}_t\right)^{-1}\triangleq\tilde{\mathbf{G}}_t^{-1}. \tag{56}$$

The covariance matrix of the posteriori estimate of dynamic state variables, which are needed to perform prediction in the next time step, can be obtained by extracting the diagonal block of $\mathbf{P}_{t(+)}$.

(7) Detection, identification, and correction of bad data. Bad data are defined as the measurements whose error exceeds the probable range of regular noise. They occur when there is a sensor malfunction, erroneous calibration, communication delay/failure, or false data injection attack [28-30].

(7.1) The normalized residuals can be obtained by dividing their absolutes value by the corresponding diagonal entry in the residual covariance matrix:

$$\tilde{\mathbf{r}}_t^{N}=\left(diag\,\tilde{\boldsymbol{\Omega}}_t\right)^{-\frac{1}{2}}\tilde{\mathbf{r}}_t, \tag{57}$$

where $\tilde{\boldsymbol{\Omega}}_t=\tilde{\mathbf{R}}_t-\tilde{\mathbf{H}}_t\left(\mathbf{x}_t\right)\left(\tilde{\mathbf{H}}_t\left(\mathbf{x}_t\right)^{T}\tilde{\mathbf{R}}_t^{-1}\tilde{\mathbf{H}}_t\left(\mathbf{x}_t\right)\right)^{-1}\tilde{\mathbf{H}}_t(\mathbf{x}_t)^{T}$ is the residual covariance matrix and $\tilde{\mathbf{r}}_t=\tilde{\mathbf{z}}_t-\tilde{\mathbf{h}}_t(\hat{\mathbf{x}}_{t(+)})$ is the residual vector.

(7.2) Find the measurement corresponding to the largest normalized residual as follows:

$$u=\arg\max_{j}\left\{\tilde{r}_t^{jN}\right\}, \tag{58}$$

where $\tilde{r}_t^{jN}$ is the j^{th} entry of vector $\tilde{\mathbf{r}}_t^{N}$.

(7.3) if $\left|\tilde{r}_t^{uN}\right|>c$, then the u-th measurement will be suspected as bad data. Correct the measurement as follows:

$$\tilde{z}_t^{u}\leftarrow\tilde{z}_t^{u}-\frac{\tilde{R}_t^{uu}}{\tilde{\Omega}_t^{uu}}\tilde{r}_t^{u}, \tag{59}$$

and return to Step (5). Otherwise, process to Step (8).

(8) Return to Step 2.

This proposed approach requires wind speed as an input. In practice, the wind speed is measured by a wind speed sensor installed at the PMSG-WT. In the case that the wind speed is unknown, a number of approaches are available to resolve the unknown input issue for DSE (please see [36-37] for example).

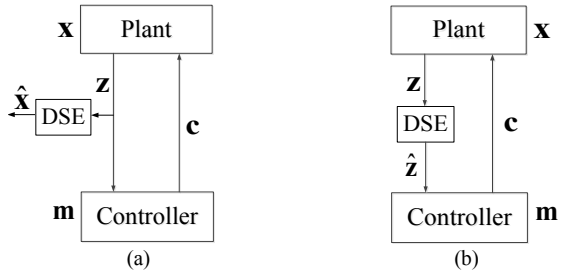

FIGURE 3. Open-loop and closed-loop operations. (a) Open-loop; (b) Closed-loop.

C. MONITORING AND CONTROL OF PMSG-WT

The plant-controller model can operate in both open-loop and closed-loop schemes for monitoring and control purposes, respectively. The system schematics under the two operation schemes are shown in Fig. 3a and 3b, respectively.

In the open-loop operation scheme shown in Fig. 3a, the DSE intakes the raw measurements $\mathbf{z}$ from the *plant*, and produces the estimated values of the PMSG-WT state variables $\hat{\mathbf{x}}$. The estimated states $\hat{\mathbf{x}}$ will be sent to the power system control center for system-wide dynamic monitoring and security assessment. In the closed-loop operation shown in Fig. 3b, the DSE intakes the raw measurements $\mathbf{z}$ from the *plant*, and sends the estimated measurements $\hat{\mathbf{z}}$ to the *controller* for real-time control of PMSG-WT. In both schemes, the DSE filters out noise, natural bad data, and malicious false data in the raw measurements, making the monitoring and control applications more effective and reliable.

Ⅳ. SIMULATION RESULTS

In order to validate the effectiveness of the proposed DSE framework in PMSG-WT monitoring and control, simulation cases in the IEEE 39-bus system will be presented in this section. It is assumed that a PMSG-WT is connected to bus 3 of the system. Both regular Gaussian noise and substantial bad data are considered in the simulations cases. The Gaussian noise includes both process noise and measurement noise. The process noise may come from model approximation and integration errors. Measurement noise may come from imperfection of the sensing process. Bad data may come from improper calibration, wrong connection, sensor failures, or cyber attacks. The DSE is carried out locally, and the sampling time is assumed to be 250 μs.

A. OPEN-LOOP OPERATION FOR MONITORING

In order to evaluate the accuracy of the proposed DSE in open-loop operation for monitoring purpose, the estimated values and the measured values of the state variables will both be compared with the true values. Fig. 4 shows the state estimation results in the presence of regular Gaussian noise. The standard deviations of the process noise and the measurement noise are set to be 10^{-5} p.u. and 10^{-3} p.u., respectively. In addition, the setpoint of the grid-side reactive power Q_{gref} has a step increase from 0 to 0.2 p.u. at 25 s.

As observed from Fig. 4, there is a short transient at the initialization stage of the simulation. Then, the system quickly enters the steady state owing to the control function. In addition, the system is also stabilized after the step change of

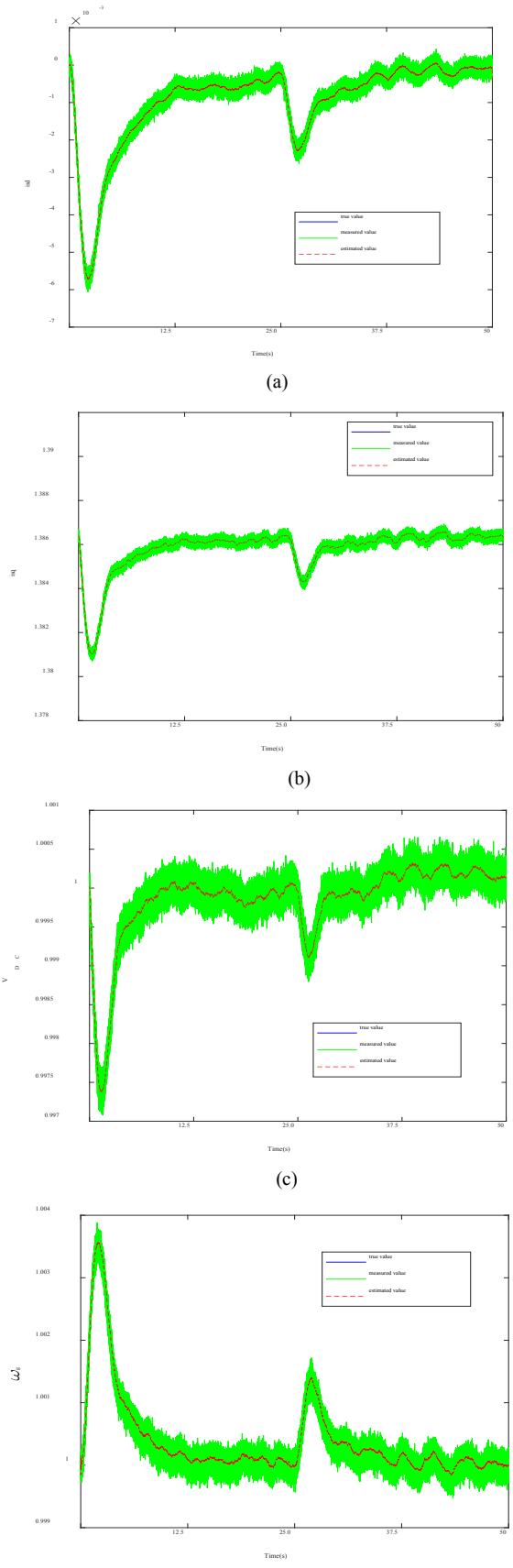

FIGURE 4. Four state variables in open-loop operation. (a) i_{sd}; (b) i_{sq}; (c) V_{DC}; (d) ω_{g} .

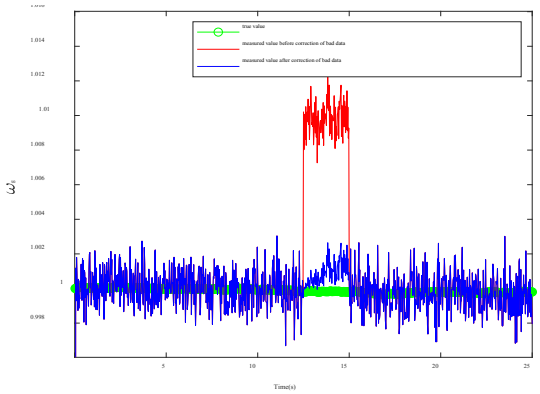

FIGURE 5. Estimation of rotor speed under bad data

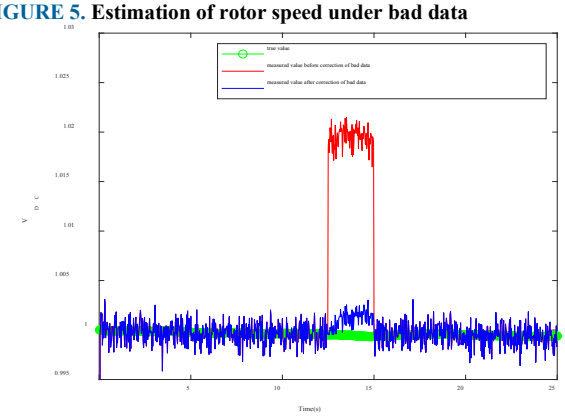

FIGURE 6. Estimation of DC-link voltage under bad data

TABLE I
RMSE_M of estimated value and measured value

RMSE_M	i_{sd}	i_{sq}	V_{DC}	ω_g
Measured	9.186×10^{-3}	9.313×10^{-3}	9.724×10^{-3}	1.128×10^{-2}
Estimated by DSE	1.975×10^{-3}	2.876×10^{-3}	1.718×10^{-3}	3.949×10^{-3}
Performance Improvement	78.49%	69.11%	72.04%	64.98%

the grid-side reactive power control setpoint. It is evident that the estimated values track the true state trajectory very well, while the measured values present substantial variations.

To quantitively verify the accuracy of DSE, a metric named the Root Mean Square Error for Monitoring (RMSE_M) is proposed. For a given variable, it computes the error of either the measured value or the estimated value with respect to the true value, as defined below:

$$\text{RMSE\_M}=\sqrt{\frac{\sum_{i=1}^{p}\sum_{j=1}^{q}(X_{obj,ij}-X_{true,ij})^2}{pq}}. \quad (60)$$

where X_{obj} represents the measured value or the estimated value of the variable, X_{true} represents the true value of the variable, p represents the number of time steps of a simulation, and q represents the number of simulations. In this case, $p = 2\times10^5$, and $q = 10$.

The RMSE_M results of four state variables are listed in Table I. Evidently the estimated values from the DSE is much more accurate than the raw measured values. Therefore, the DSE can provide much more accurate system trajectories than the raw measurements as it filters out the process noise and measurement noise.

In order to test the bad detection and correction capabilities of the proposed DSE method, in another simulation case, two sections of bad data e_a and e_b are intentionally added to corrupt the measurements. Specifically, e_a and e_b with gross errors of 0.01 p.u. and 0.02 p.u. are added to the rotor speed measurement ω_g^z and the DC-link voltage measurement V_{DC}^z from 12.5 s to 15 s, respectively. This kind of errors can be due to a natural sensor malfunction, or a malicious false data injection.

The true values, erroneous values, and corrected values of the rotor speed and the DC-link voltage are shown in Fig. 5 and Fig. 6, respectively. Evidently, the bad data from both measurements are effectively detected and corrected. Compared with the erroneous values, the corrected values closely keep track of the true values, making reliably monitoring possible under such challenging data corruption situations. Thus, it can be concluded that it is beneficial to adopt the proposed DSE instead of relying on raw measurements for system monitoring.

B. CLOSED-LOOP OPERATION FOR CONTROL

As previous described, in the closed-loop operation scheme, the DSE will pass the estimated results to the *controller*, which will in turn generate control signals for the *plant*. In order to demonstrate the improvement of control effects brought about by the proposed DSE scheme, the tracking performances of the state trajectories to the control setpoints with and without the proposed DSE in the loop will be compared. The settings of process noise and measurement noise are the same as in Section IV-A. In addition, a ramping wind speed with a slope of 1.1666667×10^{-2} m/s^2 and a Gaussian white noise of 0.002 m/s is given from 2.5 s to 12.5s.

The true trajectories of four state variables with and without DSE in the loop are presented in Fig. 7. As observed, under to transient induced by the ramp wind, the trajectories of four state variables with DSE track the corresponding control setpoints more closely than those without DSE, respectively.

In order to quantitatively verify the benefit of DSE on the control effect, a metric named Root Mean Square Error for Control (RMSE_C) is proposed. It computes the cumulative differences between the true system trajectory and the control setpoint with or without DSE in the loop, defined as follows:

$$\text{RMSE\_C}=\sqrt{\frac{\sum_{i=1}^{p}\sum_{j=1}^{q}(Y_{obj,ij}-Y_{ref,ij})^2}{pq}}. \quad (61)$$

where Y_{obj} represents the truth value of four state variables with or without DSE, Y_{ref} represents the control setpoint of four state variables, p represents the number of time steps of a simulation, and q represents the number of simulations. In this case, it is set that $p = 2\times10^5$, and $q = 10$.

The RMSE_C results of four state variables are shown in Table II. Evidently, four state variables track the control setpoints more closely when the DSE is placed into the loop. This owes to the fact that the DSE provides more accurate operation information of the *plant* to the *controller* compared with raw measurements.

Similarly as Section IV-B, in the closed-loop operation scheme, a simulation case with bad data is also performed to further demonstrate the benefit of the proposed DSE. Specifically, two bad data sections e_c and e_d with gross errors

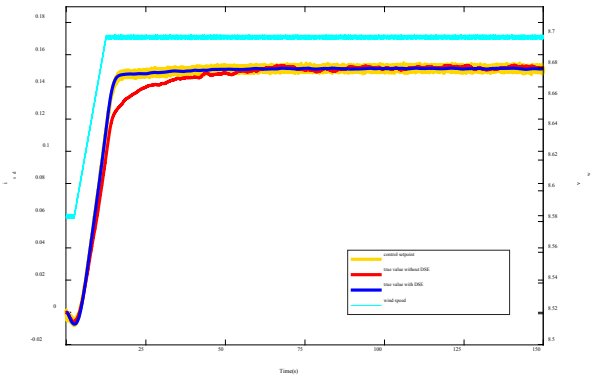

(a)

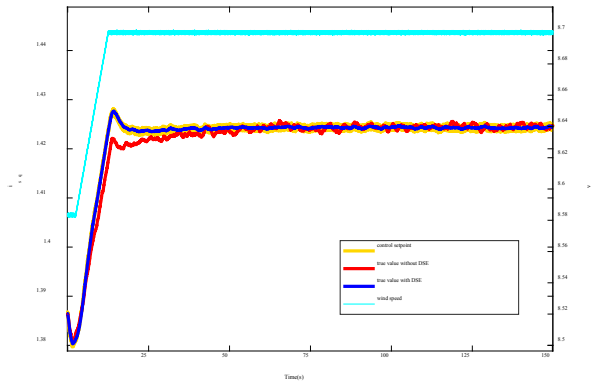

(b)

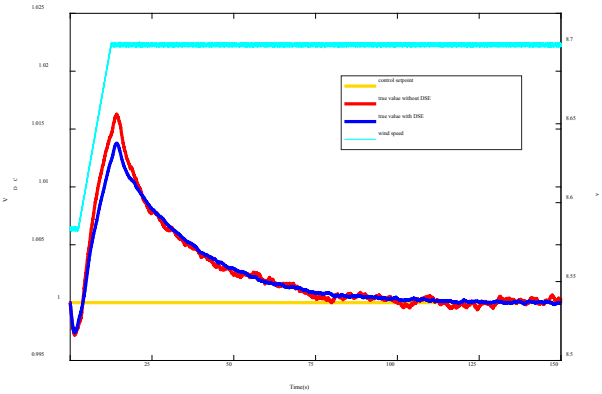

(c)

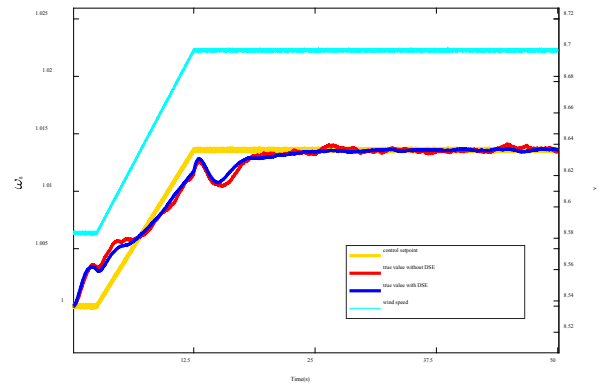

(d)

FIGURE 7. Four state variables with and without DSE. (a) i_{sd} (b) i_{sq} (c) V_{DC} (d) ω_g

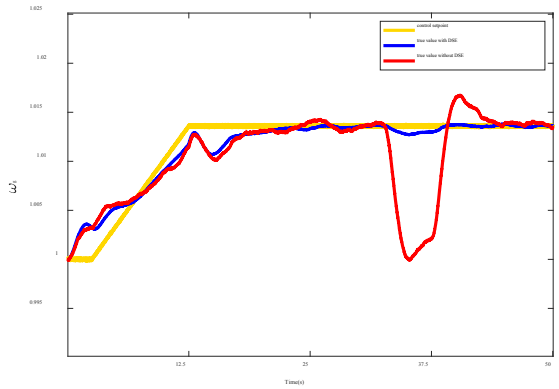

FIGURE 8. Control of rotor speed under bad data

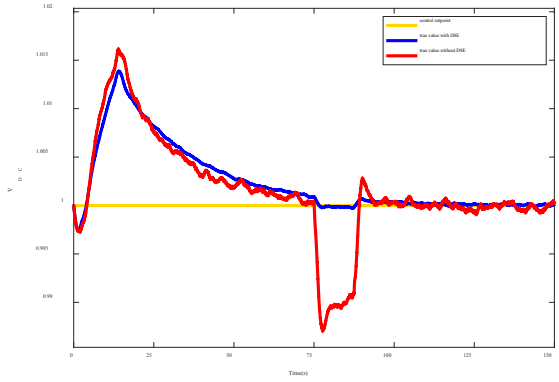

FIGURE 9. Control of DC-link voltage under bad data

TABLE II
RMSE_C with and without DSE

RMSE_C	i_{sd}	i_{sq}	V_{DC}	ω_g
Without DSE	2.874×10^{-2}	2.761×10^{-2}	1.542×10^{-2}	1.325×10^{-2}
With DSE	1.929×10^{-2}	1.823×10^{-2}	1.071×10^{-2}	0.987×10^{-2}
Performance Improvement	32.88%	33.97%	30.54%	25.51%

of 0.01 p.u. are added to the rotor speed measurement ω_g^z and DC-link voltage V_{DC}^z from 32.5 s to 37.5s and 75s to 87.5s, respectively. The control setpoint and the true state trajectories with and without the DSE are presented in Fig. 8. and Fig. 9.

As readily observed from Fig. 8 and Fig. 9, during the period when the bad data exists (i.e. from 32.5 s to 37.5 s and from 75 s to 87.5 s), the trajectories of ω_g and V_{DC}^z deviate drastically from the control setpoint without the DSE in place. This verifies the fact that bad data in measurement streams can severely impact the operation of PMSG-WTs. By contrast, in the presence of the DSE, the effect of the bad data is remarkably suppressed. The rotor speed and DC-link voltage are still able to track the control setpoint closely. This owes to the DSE's capability to detect and correct bad data. Hence, the proposed closed-loop DSE scheme allows effective control of PMSG-WTs in the presence of substantial data corruptions.

V. CONLUSION

In this paper, a general DSE framework for reliable monitoring and control of PMSG-WT is proposed. The *plant* model and

the *controller* model are separately derived to allow explicit representation of the uncertainties associated with the information exchange between them. Based on this result, a general DSE model for the physical *plant* of PMSG-WT is developed. The state transition equations and measurement equations are derived, and a WLS-form IEKF technique is presented for handling noise and bad data.

The simulation results for both the open-loop operation scheme and the closed-loop operation scheme demonstrate the effectiveness of the proposed DSE framework. In the open-loop simulation cases, it is shown that the DSE keeps track of the true state trajectories more closely than raw measurements in the presence of Gaussian noise and bad data. In the closed-loop simulation cases, it is shown that the DSE improves the performances of the *controller*, allowing tighter tracking of control setpoints in the presence of Gaussian noise and bad data compared with raw measurements. As the *plant* model and the *controller* model are decoupled, the proposed DSE framework is readily applicable to PMSG-WTs with various control paradigms.

The proposed DSE framework demonstrates the values of the technique for both monitoring and control of PMSG-WTs. In future studies, a general DSE framework for DFIG-WTs could be considered in a similar manner. It is also beneficial to investigate a general DSE framework for a wind farm consisting of a large number of wind generators.

REFERENCES

[1] E. Rebello, D. Watson and M. Rodgers, "Performance analysis of a 10 MW wind farm in providing secondary frequency regulation: experimental aspects," *IEEE Transactions on Power Systems*, vol. 34, no. 4, pp. 3090-3097, July 2019.

[2] M. Hedayati-Mehdiabadi, J. Zhang and K. W. Hedman, "Wind power dispatch margin for flexible energy and reserve scheduling with increased wind generation," *IEEE Transactions on Sustainable Energy*, vol. 6, no. 4, pp. 1543-1552, Oct. 2015.

[3] M. Rostami and S. Lotfifard, "Distributed dynamic state estimation of power systems," *IEEE Transactions on Industrial Informatics*, vol. 14, no. 8, pp. 3395-3404,Aug.2018.

[4] Y. Chen, Y. Yao, Y. Lin and X. Yang, "Dynamic state estimation for integrated electricity-gas systems based on Kalman filter," *CSEE Journal of Power and Energy Systems*, doi: 10.17775/CSEEJPES.2020.02050. (early access)

[5] S. Prasad and D. M. Vinod Kumar, "Trade-offs in PMU and IED deployment for active distribution state estimation using multi-objective evolutionary algorithm," *IEEE Transactions on Instrumentation and Measurement*, vol. 67, no. 6, pp. 1298-1307, Jun. 2018.

[6] Y. Zhang, Y. Xu and Z. Y. Dong, "Robust ensemble data analytics for incomplete PMU measurements-based power system stability assessment," *IEEE Transactions on Power Systems*, vol. 33, no. 1, pp. 1124-1126, Jan. 2018.

[7] H. Karimipour and V. Dinavahi, "Extended Kalman filter-based parallel dynamic state estimation," *IEEE Transactions on Smart Grid*, vol. 6, no. 3, pp. 1539-1549, May 2015.

[8] Ghahremani and I. Kamwa, "Local and wide-area PMU-based decentralized dynamic state estimation in multi-machine power systems," *IEEE Transactions on Power Systems*, vol. 31, no. 1, pp. 547-562, Jan. 2016.

[9] J. Zhao, M. Netto and L. Mili, "A robust iterated extended kalman filter for power system dynamic state estimation," *IEEE Transactions on Power Systems*, vol. 32, no. 4, pp. 3205-3216, July 2017.

[10] J. Zhao and L. Mili, "A theoretical framework of robust H-infinity unscented kalman filter and its application to power system dynamic state estimation," *IEEE Transactions on Signal Processing,* vol. 67, no. 10, pp. 2734-2746, 15 May15, 2019.

[11] J. Qi, K. Sun, J. Wang and H. Liu, "Dynamic state estimation for multi-machine power system by unscented kalman filter with enhanced numerical stability," *IEEE Transactions on Smart Grid*, vol. 9, no. 2, pp. 1184-1196, March 2018.

[12] W. Xie, Z. Huang, W. He and K. Wang, "A square root cubature kalman filter based dynamic state estimation of distribution network," *2020 IEEE/IAS Industrial and Commercial Power System Asia (I&CPS Asia)*, Weihai, China, 2020, pp. 497-501.

[13] A. Sharma, S. C. Srivastava and S. Chakrabarti, "A cubature kalman filter based power system dynamic state estimator," *IEEE Transactions on Instrumentation and Measurement*, vol. 66, no. 8, pp. 2036-2045, Aug. 2017.

[14] N. Zhou, D. Meng and S. Lu, "Estimation of the Dynamic States of Synchronous Machines Using an Extended Particle Filter," *IEEE Transactions on Power Systems*, vol. 28, no. 4, pp. 4152-4161, Nov. 2013.

[15] Y. Cui and R. Kavasseri, "A Particle Filter for Dynamic State Estimation in Multi-Machine Systems With Detailed Models," *IEEE Transactions on Power Systems*, vol. 30, no. 6, pp. 3377-3385, Nov. 2015.

[16] K. Emami, T. Fernando, H. H. Iu, H. Trinh and K. P. Wong, "Particle filter approach to dynamic state estimation of generators in power systems," *IEEE Transactions on Power Systems*, vol. 30, no. 5, pp. 2665-2675, Sept. 2015.

[17] T. Zhang, W. Zhang and P. Yuan, "Distributed dynamic state estimation in active distribution system based on particle filter," *2018 IEEE Innovative Smart Grid Technologies* - Asia (ISGT Asia), Singapore, 2018, pp. 664-668.

[18] M. Z. El-Sharafy, S. Saxena and H. E. Farag, "Optimal design of islanded microgrids considering distributed dynamic state estimation," *IEEE Transactions on Industrial Informatics*, vol. 17, no. 3, pp. 1592-1603, March 2021.

[19] X. Wang, X. Wei and Y. Meng, "Experiment on grid-connection process of wind turbines in fractional frequency wind power system," *IEEE Transactions on Energy Conversion*, vol. 30, no. 1, pp. 22-31, March 2015.

[20] S. Yu, K. Emami, T. Fernando, H. H. C. Iu and K. P. Wong, "State estimation of doubly fed induction generator wind turbine in complex power systems," *IEEE Transactions on Power Systems*, vol. 31, no. 6, pp. 4935-4944, Nov. 2016.

[21] S. S. Yu, J. Guo, T. K. Chau, T. Fernando, H. H. Iu and H. Trinh, "An unscented particle filtering approach to decentralized dynamic state estimation for DFIG wind turbines in multi-area power systems," *IEEE Transactions on Power Systems*, vol. 35, no. 4, pp. 2670-2682, July 2020.

[22] G. Anagnostou, L. P. Kunjumuhammed and B. C. Pal, "Dynamic state estimation for wind turbine models with unknown wind velocity," *IEEE Transactions on Power Systems*, vol. 34, no. 5, pp. 3879-3890, Sept. 2019.

[23] Saad, "Dynamic state estimation of a permanent magnet synchronous generator-based wind turbine," *IET Renewable Power Generation*, vol. 10, no. 9, pp. 1278-1286, 2016.

[24] S. Afrasiabi, M. Afrasiabi, M. Rastegar, M. Mohammadi, B. Parang and F. Ferdowsi, "Ensemble kalman filter based dynamic state estimation of PMSG-based wind turbine," *2019 IEEE Texas Power and Energy Conference (TPEC)*, College Station, TX, USA, 2019, pp. 1-4.

[25] H. Habibi, I. Howard, S. Simani and A. Fekih, "Decoupling adaptive sliding mode observer design for wind turbines subject to simultaneous faults in sensors and actuators," *IEEE/CAA Journal of Automatica Sinica*, vol. 8, no. 4, pp. 837-847, April 2021.

[26] H. W. Sorenson, "Least-squares estimation: from Gauss to Kalman," *IEEE Spectrum*, vol. 7, no. 7, pp. 63-68, Jul. 1970.

[27] J. Zhao, M. Netto and L. Mili, "A robust iterated extended kalman filter for power system dynamic state estimation," *IEEE Transactions on Power Systems*, vol. 32, no. 4, pp. 3205-3216, July 2017.

[28] A. Abur and A. Gómez-Expósito, *Power System State Estimation: Theory and Implementation*. New York, NY, USA: Marcel Dekker, 2004.

[29] Y. Lin and A. Abur, "A highly efficient bad data identification approach for very large scale power systems," *IEEE Transactions on Power Systems*, vol. 33, no. 6, pp. 5979-5989, Nov 2018.

[30] Z. Li, J. Liu, Y. Lin, and F. Wang, "Grid-Constrained Data Cleansing Method for Enhanced Bus Load Forecasting", *IEEE Transactions on Measurement and Instrumentation*. (early access)

[31] L. Chen *et al*., "Study of a modified flux-coupling-type SFCL for efficient fault ride-through in a PMSG wind turbine under different types of faults," *Canadian Journal of Electrical and Computer Engineering*, vol. 40, no. 3, pp. 189-200, Summer 2017.

[32] Z. Zhang, Y. Zhao, W. Qiao and L. Qu, "A discrete-time direct torque control for direct-drive PMSG-based wind energy conversion systems,"

IEEE Transactions on Industry Applications, vol. 51, no. 4, pp. 3504-3514, July-Aug. 2015.

[33] M. F. M. Arani and Y. A. I. Mohamed, "Assessment and enhancement of a full-scale PMSG-based wind power generator performance under faults," *IEEE Transactions on Energy Conversion*, vol. 31, no. 2, pp. 728-739, June 2016.

[34] B. Wu, Y, Lang, N. Zargari, K. Samir, *Power Conversion and Control of Wind Energy Systems*. IEEE Press, Wiley, 2011.

[35] C. Wei, Z. Zhang, W. Qiao and L. Qu, "An adaptive network-based reinforcement learning method for MPPT control of PMSG wind energy conversion systems," *IEEE Transactions on Power Electronics*, vol. 31, no. 11, pp. 7837-7848, Nov.2016.

[36] Hamed Habibi, Hamed Rahimi Nohooji, and Ian Howard, "Optimum efficiency control of a wind turbine with unknown desired trajectory and actuator faults", *Journal of Renewable and Sustainable Energy* vol. 9, 063305, 2017.

[37] E. Ghahremani and I. Kamwa, "Dynamic state estimation in power system by applying the extended Kalman filter with unknown inputs to phasor measurements," *IEEE Transactions on Power Systems*, vol. 26, no. 4, pp. 2556-2566, Nov. 2011.

Shaojian Song received the B.S., and M.S. degrees from Guangxi University, Nanning, China, in 1994 and 2001 respectively. Since 1994, he has been with school of Electrical Engineering at Guangxi University, where he became Professor in 2010. He visited New York State Center for Future Energy Systems at Rensselaer Polytechnic Institute, USA, from 2014 to 2015.His current research interests include power electronics and energy conversion, active distribution networks, state estimation, optimal control and machine learning.

Panzhou Wu received his B.S. degree in Electrical Engineering and Automation from Southwest University for Nationalities, Chengdu, China, in 2018. He is currently pursuing his M.S. degree in Control Science and Engineering at Guangxi University, Nanning, China. His research interests include state estimation of power systems with renewable energy.

Yuzhang Lin (M'18) is currently an Assistant Professor in the Department of Electrical and Computer Engineering at the University of Massachusetts, Lowell, MA, USA. He obtained his Bachelor and Master's degrees from Tsinghua University, Beijing, China, and Ph.D. degree from Northeastern University, Boston, MA, USA. His research interests include smart grid modeling, monitoring, data analytics, and cyber-physical resilience. He is currently serving as an Editor for CSEE Journal of Power and Energy Systems.

Yanbo Chen (M'13, SM'20) received the B.S., the M.S. and the Ph.D. degrees in electrical engineering from Huazhong University of Science and Technology, China Electric Power Research Institute, Tsinghua University, in 2007, 2010 and 2013, respectively. He is currently an associate professor of North China Electric Power University. His research interests include state estimation and power system analysis and control. He is an Associate Editor of IEEE Access.